

Supplemental Materials

Biallelic Cys141Tyr variant of *SEL1L* is associated with neurodevelopmental disorders, agammaglobulinemia and premature death

Denisa Weis^{1,2,14*}, Lianguang Leo Lin^{3,4,14}, Huilun Helen Wang^{3,4,14}, Zexin Jason Li^{3,5}, Katarina Kusikova⁶, Peter Ciznar², Hermann Maximilian Wolf^{7,8}, Alexander Leiss-Piller⁷, Zhihong Wang^{3,4}, Xiaoqiong Wei^{3,4}, Serge Weis⁹, Katarina Skalicka², Gabriela Hrckova², Lubos Danisovic¹⁰, Andrea Soltysova^{11,12}, Tingxuan Tina Yang⁴, René Günther Feichtinger^{14,17}, Johannes Adalbert Mayr^{13,15*}, Ling Qi^{3,4,5,15,16*}

Contents:

- Methods
- Supplemental Tables 1-3
- Supplemental Figures 1-10

METHODS

Genetic analysis

The informed consent was obtained from the parents of the patient and this study was approved by Johannes Kepler University Ethics Committee (Approval No: 1253/2021). The venous blood samples were collected for genomic DNA extraction from individual (III-3, III-4, IV-4 and IV-6).

The Human Genome CGH Microarray (4x44K Agilent Technologies, USA) designed with enhanced coverage on known genes (24 Kb) were performed in Patients 3 and 5, and parents. Subsequently, SurePrint G3 Human Genome CGH+SNP 2x400K Microarray was performed in Patients 3 and 5, to increase the resolution with the median spacing of 4.5 Kb in Refseq genes. Appropriate sex-matched samples included in SureTag Complete DNA Labeling Kit (Agilent Technologies, USA) were used as references. DNA labeling, hybridization and washing were performed according to the manufacturer's protocols (Agilent). Microarray slides were scanned using SureScan Microarray Scanner. Data were analyzed with default algorithm settings using Cytogenomics Software (Agilent Technologies, USA). Pathogenicity of all identified CNVs variants was verified in the UCSC Genome Browser, Database of Genomic Variants (DGV), International Standards for Cytogenomic Arrays (ISCA) database and DECIPHER.

Whole exome sequencing was performed using the human comprehensive exome 37Mb (Twist Bioscience, USA) on an Illumina NovaSeq SP flow cell, 2x150bp PE sequencing (Illumina, USA). Data analysis was performed using CLC Genomics Workbench 9.5.2 (QIAGEN, Germany). Reads were trimmed by quality (limit 0.05), and by ambiguous nucleotides (limit 3). Trimmed reads were then mapped against the human genome (GRCh37 / hg19; match score 1, mismatch cost 2, insertion and deletion cost 3, length fraction 0.5 and similarity fraction 0.8, non-specific match handling was set to map randomly) and locally realigned (multi-pass realignment 3). Variants were called using the low frequency variant detection tool (required significance 1%, minimum coverage 10, minimum count 2, minimum frequency 1%, base quality filter with neighborhood radius 5, minimum central quality 20, and minimum neighborhood quality 15, direction and position filters with direction frequency 5%, relative read direction filter significance 1%, and read position filter significance 1%). Called variants were then processed for storage in a database (MariaDB 10.1, MariaDB Corporation, USA). Variants were annotated using the Ensemble variant effect predictor (VEP) tool (1) and also separately the combined annotation dependent depletion (CADD) tool (2). VEP annotated variants were then filtered against their allele frequency (AF): variants having AF>1% in any (sub-) population were filtered

out and only variants with $AF \leq 1\%$ or unknown AF were further processed. Remaining variants were then filtered against their CADD PHRED score (≥ 10) and affected genes were annotated by HGNC multi-symbol checker, UniProtKB, and OMIM. Genes were also queried for pathway involvement by reactome (3), for gene-gene interactions by string-db (4), and gene expression by BioGPS (5), and Bgee (doi 10.1007/978-3-540-69828-9_12).

Skin biopsy and primary fibroblasts culture

Skin biopsies was performed on Patient 5 (IV-6) as described (6). Skin fibroblast cell lines were established in RPMI medium supplemented with 20% fetal bovine serum (FBS) and 1% penicillin/streptomycin (P/S) (Thermo Fisher Scientific) at 37°C in a humidified atmosphere with 5% CO₂. Cell lines were maintained in an incubator set to 37°C and 5% CO₂ and cultured in DMEM with high glucose, GlutaMAX™, and pyruvate (ThermoFisher, 31966-021), supplemented with 10% FBS and 50 µg/ml uridine (Sigma), or DMEM with glutamine, w/o glucose and w/o pyruvate (ThermoFisher, 11966-025) supplemented with 0.3 mM β-hydroxybutyrate (Cayman Chemical, 14148), 10% FBS, and 1% P/S for 24 hr. Cells were regularly screened for and confirmed free mycoplasma using the MycoAlert Lonza kit (Lonza, LT07-418) or the Look Out Mycoplasma PCR Detection Kit (Sigma, MP0035). Cells were treated with 50 µg/ml Cycloheximide (CHX) for the indicated time points, or 40 µg/ml Chloroquine (CQ) or 10 µM MG132 for 2 hr followed by western blot analysis.

Immunological profile and Flow-cytometric Assay for Specific Cell-mediated Immune response in Activated whole blood (FASCIA)

Immunophenotyping was performed using flow cytometry as previously described (7), with the following antibodies: anti-CD3 (Invitrogen, #7D6; BD, #UCHT1), anti-CD4 (BD, #RPA-T4), anti-CD8 (BD, #RPA-T8), anti-CD16 (BD, #3G8), anti-CD19 (BD, #4G7), anti-CD20 (Miltenyi Biotec, #LT20), anti-CD25 (BD, #MA-251), anti-CD27 (Sony, #O323; BD, #L128), anti-CD45RA (BD, #HI100;), anti-IgA (Miltenyi Biotec, #IS11-8E10), anti-IgG (BD, #G18-145), anti-IgM (Miltenyi Biotec, #PJ2-22H3), anti-NKG2A (Miltenyi Biotec, #REA110), anti-NKG2C (Miltenyi Biotec, #REA205) and anti-TCR-iNKT (BD, #6B11). FASCIA test for cell proliferation was used to determine the immune response to SARS-CoV-2 based on previous publication (8).

Immunohistochemistry

Duodenum samples of patient 3 and samples with inconspicuous cases or other intestinal disorders (Supplemental Table 3) were used for immunohistochemistry staining.

Immunohistochemistry was performed on formalin-fixed and paraffin-embedded (FFPE), 5 µm-thick sections on Superfrost Plus Adhesion Microscope slides (EpreDia, #J1800AMN2). The slides were heated for 1 h at 60°C. After rehydration (4 min xylol for three times, 3 min isopropanol for three times), the slides were washed 3 min in ddH₂O for three times (3 x). Heat-induced antigen retrieval was performed in 1 mM EDTA, 0.05% Tween-20, pH 8.0 for 40 min at 95°C. Slides were allowed to cool down to room temperature. After washing 3 x 3 min in ddH₂O and 3 x 3 min in PBST (136 mM NaCl, 2,7 mM KCl, 8 mM Na₂HPO₄, 1,4 mM KH₂PO₄; 5 ml Tween-20 per liter of PBS), the endogenous peroxidase activity was blocked with peroxidase block (DAKO envision kit) for 5 min. The slides were washed 3 x 3 min in PBST. For IHC, the following antibodies were used for immunohistochemical staining for 1 hr at room temperature: anti-SEL1L (St John's Laboratory, #STJ113972, 1:100), anti-HRD1 (Proteintech, #13473-1-AP, 1:100), anti-OS9 (Cell Signaling, #12497, 1:100), anti-CD20 (Ventana, #L26, ready-to-use), anti-CD3 (Ventana, #2GV6, ready-to-use), anti-CD4 (Ventana, # SP35, ready-to-use), anti-CD8 (Ventana, #SP57, ready-to-use). All antibodies were diluted in Dako antibody diluent with background-reducing components (Dako, Glostrup, Denmark). After washing 3 x 3 min in PBST, the slides were incubated with the respective DAKO polymer (rabbit or mouse) for 1 hr at room temperature. After washing 3 x 3 min in PBST, DAB development was performed. Samples were rinsed 5 min in tap water to stop the reaction. Nuclei were stained with hemalaun for 3-5 min, briefly rinsed in 3% HCL-EtOH and bluing was done for 10 min in running tap water. After dehydration in isopropanol and xylol mounting was done in Histokit. The images were taken with a 100x magnification. Alternatively, IHC was carried out using the BenchMark ULTRA (Ventana, UK) and the UltraView DAB Kit (Ventana, UK). Sections were deparaffinized automatically by the immunostainer. Antigen demasking was performed using the ULTRA cell Conditioning 1 (Ventana, UK). After application of the primary antibody, counterstaining was done using hematoxylin followed by a bluing step.

Immunofluorescence

Human primary skin fibroblasts were seeded to a maximum of 50% confluency on culture slides. After overnight fixation in neutral buffered 4% formaldehyde solution at 4°C cells were washed 3 x 3 min in PBS. Samples were then blocked by using blocking buffer (5% Donkey serum, 0.3% Triton-100 in PBS) for 1 hour. First antibodies were diluted in dilution buffer (5% Donkey serum, 0.1% Triton-100 in PBS) at the following dilutions: anti-SEL1L (home-made, 1:400), anti-HRD1 (Proteintech, #13473-1, 1:200), anti-KDEL (Novus Biologicals, #NBP1-97469, 1:250) and incubated at 4°C overnight. After washing 3 x 3 min with PBS, the slides were incubated for 1 hr

at room temperature with Alexa Fluor Plus 555 donkey anti-mouse IgG (Thermo Scientific, #A32773, 1:500) and/or Alexa Fluor 647 anti-rabbit IgG (Jackson ImmunoResearch, #711-605-152, 1:500). The slides were mounted with ProLong Diamond Antifade Mountant with DAPI (Invitrogen, # P36965). Images were taken with Leica STELLARIS 8 FALCON confocal Microscope via University of Michigan Microscopy and Imaging Analysis Core (MIAC) Michigan Diabetes Research Center.

Protein structure modeling and sequence alignment

The individual structure models of human SEL1L, HRD1, OS9, and DERLIN1 were downloaded from AlphaFold2 database (<https://alphafold.ebi.ac.uk/>) (9). The complex structure was constructed using TM-align (10) by superposing the predicted human SEL1L, HRD1, OS9, and DERLIN1 structures to the CryoEM structure of the yeast Hrd3p-Hrd1p-Der1p protein complex (PDB ID: 6VJZ) and Hrd3p-Yos9 complex (PDB ID: 6VK3). All the structure images of human SEL1L residues 171-723, HRD1 1-334, OS9 33-655 and DERL1 1-213 were rendered by PyMOL (version 2.3.2). To analyze the evolutionary conservation of different amino acids on each site, a position-specific scoring matrix (PSSM) was generated for each protein from a PSI-BLAST search of the target protein through the NCBI NR database (11, 12). The amino acid sequence of human SEL1L (accession no. NP_005056.3) was aligned with the SEL1L homologs from chimpanzee (JAA44458.1), gibbon (XP_003260889.1), marmoset (XP_002754215.1), dog (XP_038530327.1), rabbit (XP_002719662.2), hamster (NP_001268291.1), mouse (NP_001034178.1), bird (XP_021143193.1), frog (XP_041430335.1), bony fish (NP_001038629.1), shark (XP_048393621.1), drosophila (NP_001262882.1) and yeast (QHB10358.1) by using ClustalW program.

Immunoprecipitation (IP)

HEK293T cells transfected with the indicated plasmids were snap-frozen in liquid nitrogen and whole cell lysate was prepared in IP lysis buffer [150 mM NaCl, 0.2% Nonidet P-40 (NP40), 0.1% Triton X-100, 25 mM Tris-HCl pH 7.5] at 4°C, supplemented with protease inhibitors, protein phosphatase inhibitors, and 10 mM N-ethylmaleimide. A total of ~5 mg protein lysates were incubated with 10 µl anti-FLAG agarose (Sigma, #A2220) overnight at 4°C with gentle rocking. The incubated agaroses were washed with IP lysis buffer for three times and eluted in SDS sample buffer at 95°C for 5 min followed by SDS-PAGE and Immunoblot.

RNA preparation and RT-PCR

Total RNA was extracted from cells using TRI Reagent and BCP phase separation reagent (Molecular Research Center, TR 118). RT-PCR primer sequences are:

hSEL1L F: 5'-AAACCAGCTTTGACCGCCAT-3' R: 5'-GTCATAGGTTGTAGCACACCAC-3'

hHRD1 F: 5'-CCTGCGTAACATCCACACAC R: 5'-TCTGAGCTAGGGATGCTGGT-3'

hOS9 F: 5'-CAGCGTGAAAGGGAGGAGGAAA R: 5'-GTGGTATTGCTGGATGTGGCGT-3'

hERLEC1 F:5'-CAAGTGGGGATGAGGAAGAAGA-3' R: 5'-CATGGTACTGCCGAATGTGTTT-3'

hXBP1: F: 5'-GAATGAAGTGAGGCCAGTGG-3' R: ACTGGGTCCTTCTGGGTAGA

hL32 F: 5'-AGTTCCTGGTCCACAACGTC-3' R: 5'-TTGGGGTTGGTGACTCTGAT

REFERENCES

1. McLaren W, Gil L, Hunt SE, Riat HS, Ritchie GR, Thormann A, et al. The Ensembl Variant Effect Predictor. *Genome Biol.* 2016;17(1):122.
2. Rentzsch P, Witten D, Cooper GM, Shendure J, and Kircher M. CADD: predicting the deleteriousness of variants throughout the human genome. *Nucleic Acids Res.* 2019;47(D1):D886-D94.
3. Gillespie M, Jassal B, Stephan R, Milacic M, Rothfels K, Senff-Ribeiro A, et al. The reactome pathway knowledgebase 2022. *Nucleic Acids Res.* 2022;50(D1):D687-D92.
4. Szklarczyk D, Gable AL, Nastou KC, Lyon D, Kirsch R, Pyysalo S, et al. The STRING database in 2021: customizable protein-protein networks, and functional characterization of user-uploaded gene/measurement sets. *Nucleic Acids Res.* 2021;49(D1):D605-D12.
5. Wu C, Macleod I, and Su AI. BioGPS and MyGene.info: organizing online, gene-centric information. *Nucleic Acids Res.* 2013;41(Database issue):D561-5.
6. Kaiyrzhanov R, Mohammed SEM, Maroofian R, Husain RA, Catania A, Torracco A, et al. Bi-allelic LETM1 variants perturb mitochondrial ion homeostasis leading to a clinical spectrum with predominant nervous system involvement. *Am J Hum Genet.* 2022;109(9):1692-712.
7. Beziat V, Tavernier SJ, Chen YH, Ma CS, Materna M, Laurence A, et al. Dominant-negative mutations in human IL6ST underlie hyper-IgE syndrome. *J Exp Med.* 2020;217(6).
8. Lind Enoksson S, Bergman P, Klingstrom J, Bostrom F, Da Silva Rodrigues R, Winerdal ME, et al. A flow cytometry-based proliferation assay for clinical evaluation of T-cell memory against SARS-CoV-2. *J Immunol Methods.* 2021;499:113159.
9. Jumper J, Evans R, Pritzel A, Green T, Figurnov M, Ronneberger O, et al. Highly accurate protein structure prediction with AlphaFold. *Nature.* 2021;596(7873):583-9.

10. Zhang Y, and Skolnick J. TM-align: a protein structure alignment algorithm based on the TM-score. *Nucleic Acids Res.* 2005;33(7):2302-9.
11. Altschul SF, Madden TL, Schaffer AA, Zhang J, Zhang Z, Miller W, et al. Gapped BLAST and PSI-BLAST: a new generation of protein database search programs. *Nucleic Acids Res.* 1997;25(17):3389-402.
12. Sayers EW, Bolton EE, Brister JR, Canese K, Chan J, Comeau DC, et al. Database resources of the national center for biotechnology information. *Nucleic Acids Res.* 2022;50(D1):D20-D6.

SUPPLEMENTAL TABLE**Supplemental Table 1. Prioritized variants from Whole Exome Sequencing data**

	FAR2	SEL1L
<i>Full name</i>	fatty acyl-CoA reductase 2	suppressor/enhancer of Lin-12-like, or SEL1L adaptor subunit of ERAD E3 ubiquitin ligase
<i>Chromosome</i>	12	14
<i>Position (GRch37)</i>	29,486,647	81,972,504
<i>nucleotide reference</i>	C	C
<i>nucleotide alteration</i>	T	T
<i>cDNA</i>	1468C>T	422G>A
<i>Protein</i>	Arg490Trp	Cys141Tyr
<i>dbSNP153</i>	rs767224864	
<i>gnomAD_exomes_AF</i>	0.00002477	
<i>CADD_phred</i>	24.8	29.3
<i>PolyPhen2-HVAR_pred</i>	probably damaging	probably damaging
<i>SIFT_pred</i>	damaging	damaging
<i>ConDel</i>	deleterious	deleterious
<i>Provean</i>	deleterious	neutral

Supplemental Table 2. Clinical feature of patients.

	Patient 1 (IV-1)	Patient 2 (IV-2)	Patient 3 (IV-3)	Patient 4 (IV-5)	Patient 5 (IV-6)
Date of birth (MM/YY)	Jul-06	Aug-14	Oct-09	Jul-14	Mar-16
Time of last visit (MM/YY)	May-09	Oct-14	Jul-12	Mar-22	Feb-21
Time of decease (MM/YY)	Sep-09	Oct-14	Jul-12	Mar-22	Apr-21
Sex	F	F	M	F	M
Ethnicity	European				
Consanguinity	+				
Early death at	2.9 years	2 months	2.5 years	7.9 years	5.1 years
Intellectual disability	Severe, no words	No eye contact	Severe, no words	Severe, no words	Severe, no words
Hypotonia /Ataxia	Severe axial hypotonia	Severe axial hypotonia	Severe axial hypotonia	Severe axial hypotonia	Severe axial hypotonia
Ataxia	No	NA	No	No	No
Developmental milestones delay	Global developmental delay, any motor milestones, no speech	NA	Global developmental delay, no speech	Severe global developmental delay (in age 4.5 years can turn, sit with support, tries to stand with support, no speech)	Severe global developmental delay (any motor milestones, no speech)
Short stature	(-3.28 SD)	NA	(-2.62 SD)	(-3.12 SD)	(-2.25 SD)
Underweight	(-5.81 SD)	NA	(-4.21 SD)	(-3.03 SD)	(-2.64 SD)
Microcephaly	(-1.89 SD)	NA	Normal	(-2.83 SD)	(-2.64 SD)
Seizures	No epileptic seizure	No epileptic seizure	Epilepsy nonspecific/West syndrome valproat therapy	No epileptic seizure	No epileptic seizure
Facial dysmorphisms	Palpebral ptosis	ND	Palpebral ptosis, pointed chin, full cheeks, big ears	Palpebral ptosis, thin upper lip, pointed chin, full cheeks, big ears	Palpebral ptosis, thin upper lip, pointed chin, full cheeks, big ears
Brain imaging abnormalities	MRI normal myelinization	ND	MRI normal myelinization	MRI at 10 months of age unspecific leukoencephalopathy	MRI at 1 year of age leukoencephalopathy frontal, parietal and

				frontal and occipital bilaterally	occipital bilaterally age 4.5 y discrete subtentorial cortical atrophy
EEG abnormalities	ND	ND	Slow basic activity in the delta-theta band, repeated finding of higher theta waves in the posterior leads, without specific epileptiform changes.	ND	ND
Blood tests	Respiratory insufficiency - hypercapnia	ND	Sideropenic anemia	Sideropenic anemia, increased folate level and hypovitaminosis D	Chronic respiratory insufficiency hypercapnia, sideropenic anemia
Eye symptom	Palpebral ptosis	ND	Bilateral partial papillary atrophy, Glaucoma cong.	Ptosis, bilateral partial papillary atrophy	Palpebral ptosis bilateral papillary excavation
Immunity	Agammaglobulinemia since birth	ND	Agammaglobulinemia since birth	Agammaglobulinemia since birth	Agammaglobulinemia since birth
Miscellaneous	State after acute renal failure, pulmonary hypertension	Severe bronchopneumonia	Ventricular septal defect, pectus excavatum, alopecia areata, thin brittle hair, micropenis, celiac disease		Micropenis, central hypothyreosis, hypoplastic thymus, hepatopathy, dystrophic nails

NA, Not applicable; ND, Not detected.

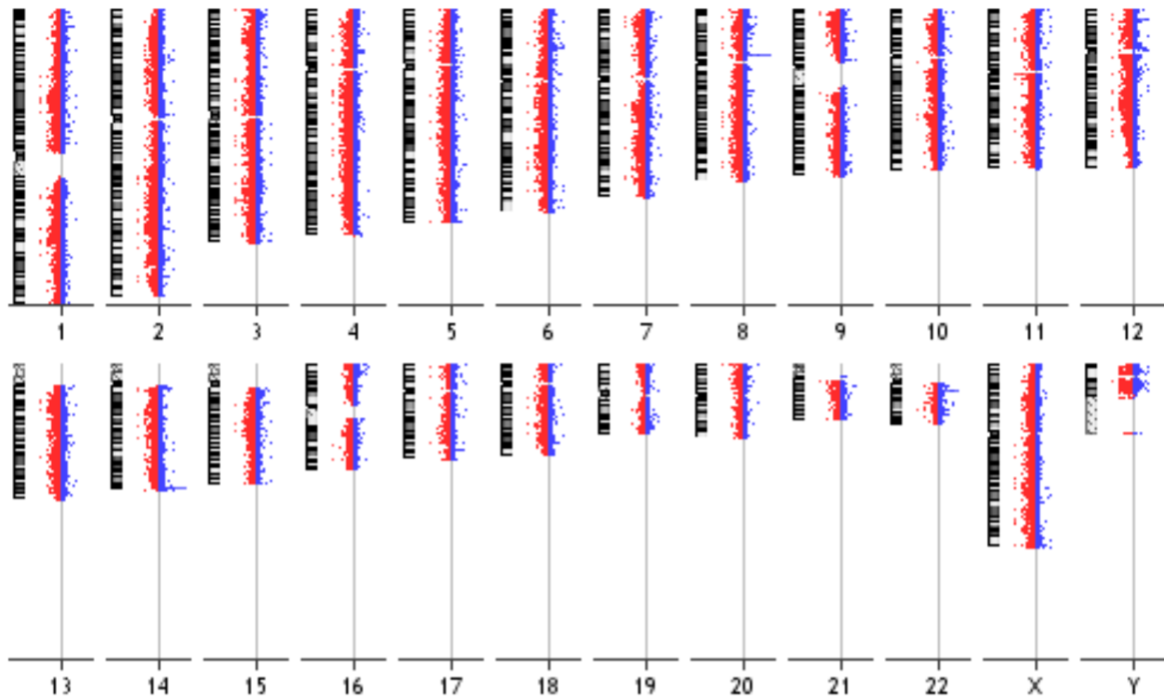
Supplemental Table 3. Evaluation of B cell and T cell number in control and patient gut samples

Case ID	Age	Sex	Diagnosis	CD3*	CD4	CD8	CD20
Patient 3 (IV-3)	2.9	M	N/A	3	2	3	0
10498	5.3	M	Coeliac disease IIIb	3	3	3	1
9626	6.7	F	Coeliac disease I	3	3	3	1
10291	10.3	F	Duodenitis	2	2	2	0
2488	0.6	F	Duplication	2	2	2	1
6392	3.3	M	Inconspicuous	2	2	2	0
15441	2.8	F	edema	2	2	2	1
7954	2.3	F	Inconspicuous	2	3	2	0

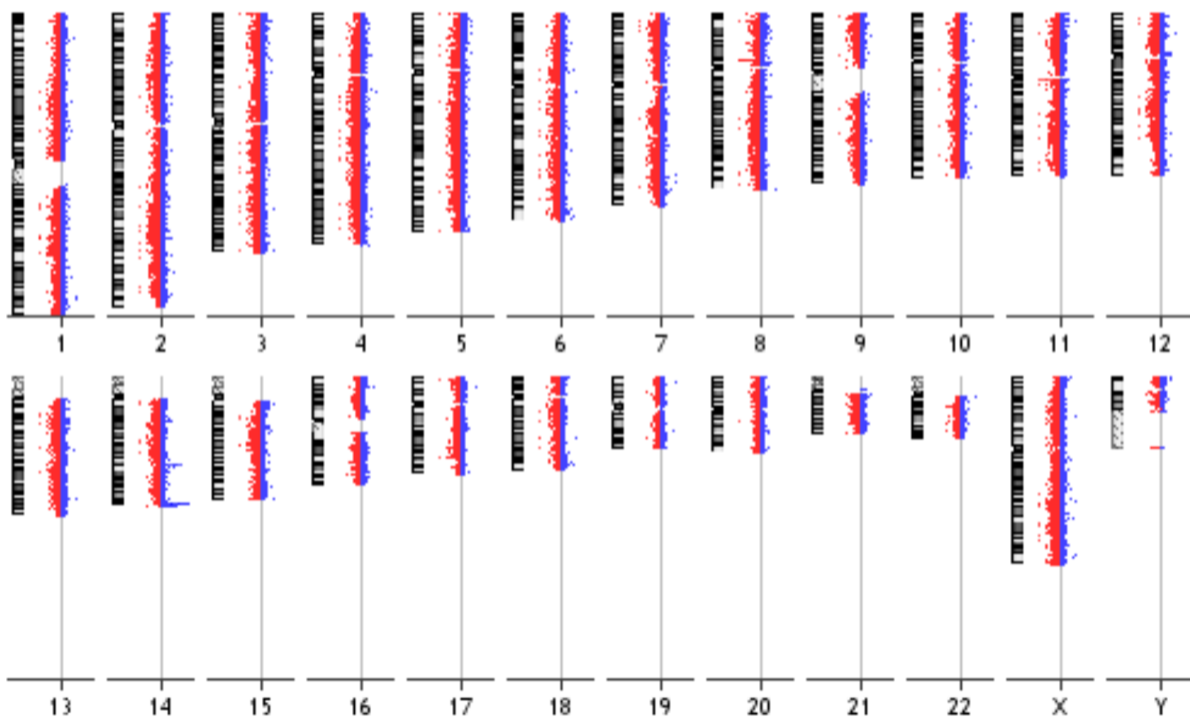
* Rating criteria: 0: no cell stained. 1: low number of cells stained 2: moderate number of cells stained. 3: high number of cells stained.

SUPPLEMENTAL FIGURES AND FIGURE LEGENDS

Patient 4



Patient 5

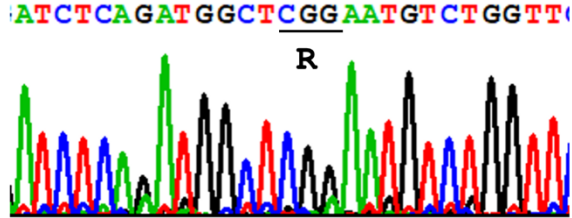


Supplemental Figure 1. aCGH data analysis of *SEL1L*^{C141Y} patients.

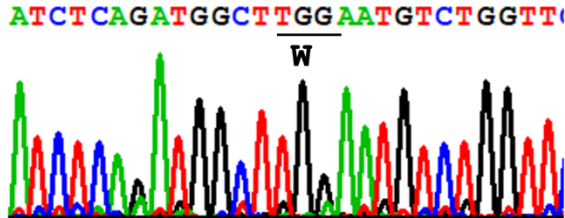
aCGH data were collected for Patients 4 and 5, showing no large chromosomal deletion or amplification. Chromosomal maps were shown on the left of each chromosomal array results. Red dots indicate control DNA signal, and blue dots indicate patient's DNA signal. The balance of control and patient signals indicates no copy number gain or loss.

FAR2 c.1468C>T; p.Arg490Trp

IV-2 (Patient 2) WT

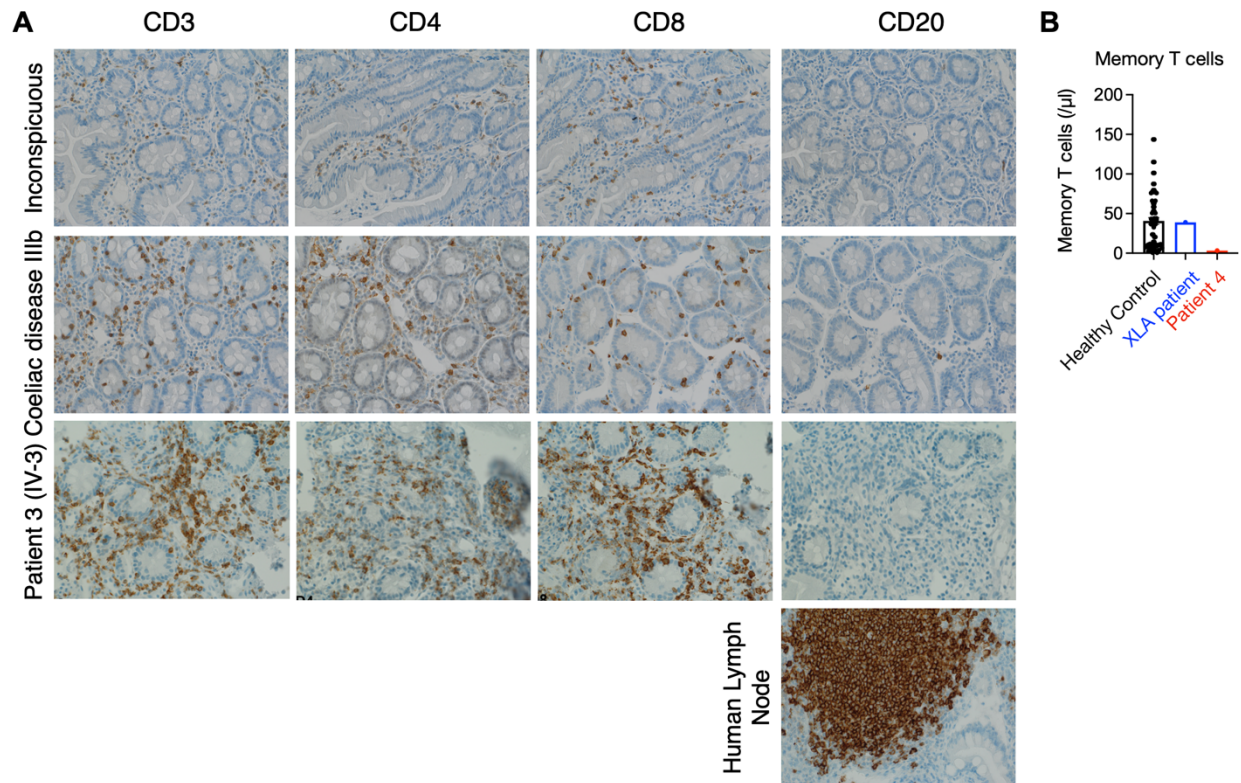


IV-5 (Patient 4) Homozygous

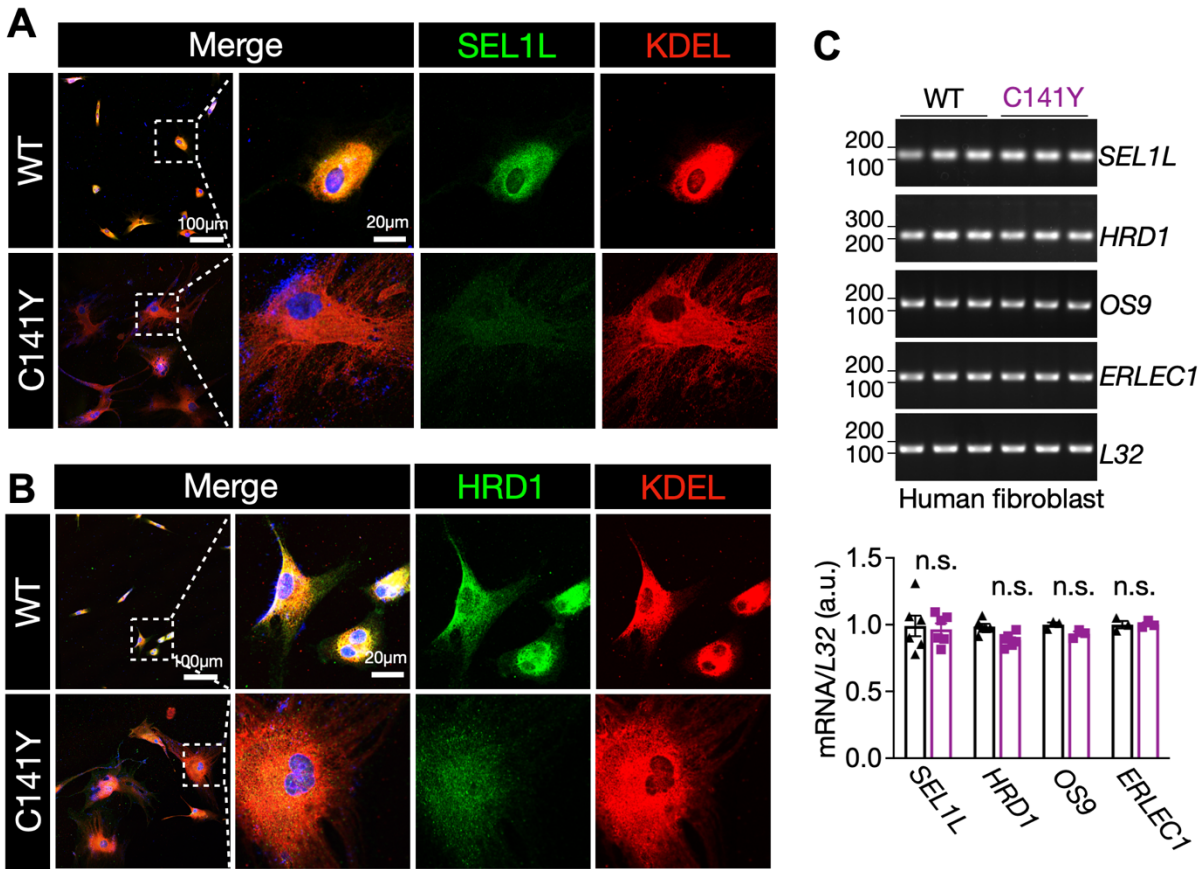


Supplemental Figure 2. Segregation analysis of *FAR2* c.1468C>T variants by Sanger sequencing.

Sanger sequencing results of *FAR2* in Patients 2 and 4.

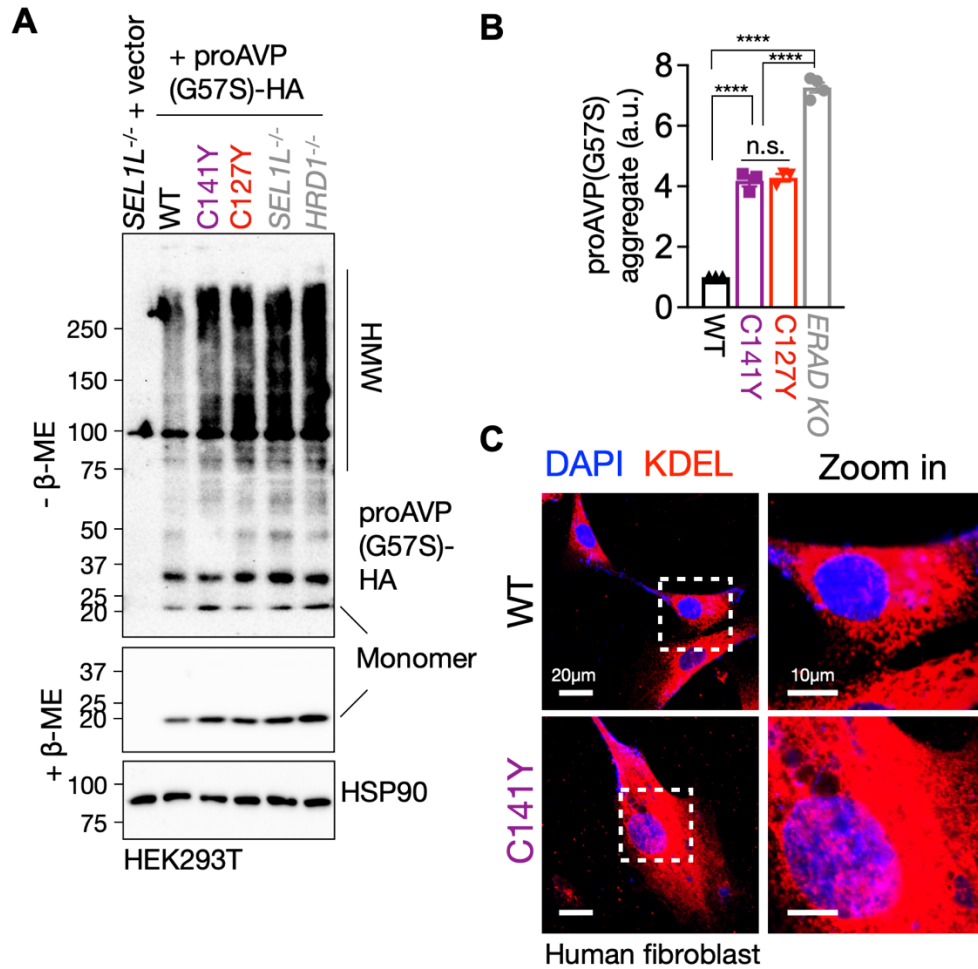


Supplemental Figure 3. The intestinal biopsy and post COVID-19 memory T cells number of ENDI-A patient. (A) Immunohistochemical staining of B and T cell markers in the duodenal biopsies from the patients diagnosed with inconspicuous (Male at age of 3.3 years old) and Coeliac disease IIIb (Male at age of 5.3 years old), and our patient 3 (IV-3). Immunohistochemical staining of B cell in a lymph node in human duodenal biopsy was used as a positive control. The images were taken under 40X magnification. **(B)** Number of COVID antigen-specific memory T cells in healthy control children, XLA patient and patient 4 at age of 7 years old post COVID-19 infections.

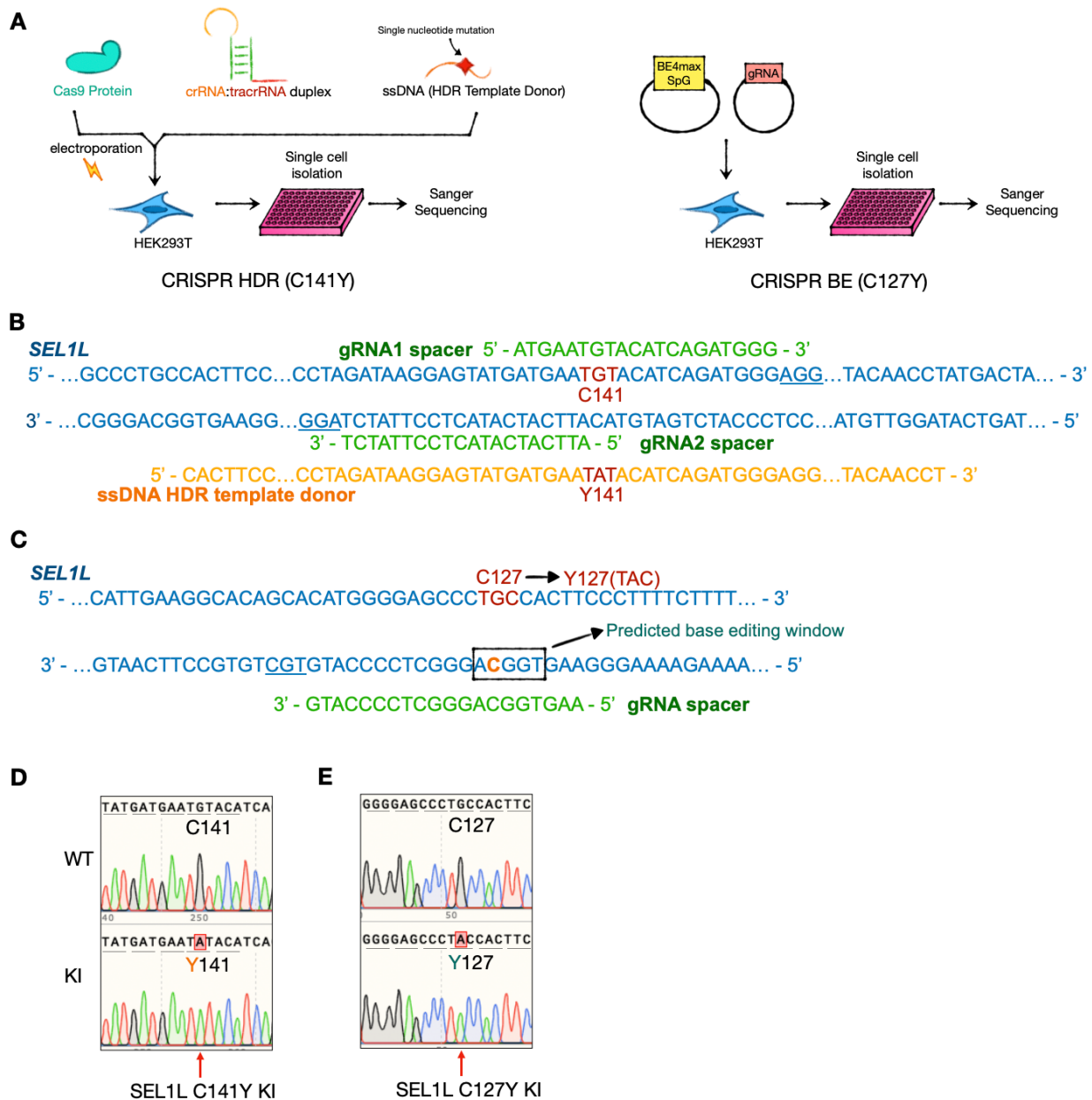


Supplemental Figure 4. *SEL1L*^{C141Y} reduces ERAD expression.

(A-B) Representative confocal microscopic images of SEL1L (A) and HRD1 (B) co-stained with KDEL in WT and *SEL1L*^{C141Y} patient fibroblasts. Blue, DAPI. (C) RT-PCR analysis of *SEL1L*, *HRD1*, *OS9* and *ERLEC1* transcript levels in WT and *SEL1L*^{C141Y} patient fibroblasts with quantitation shown on below (n = 3-6 individual experiments per group). Data are presented as mean ± SEM. n.s., not significant, by two-tailed Student's *t*-test (C).

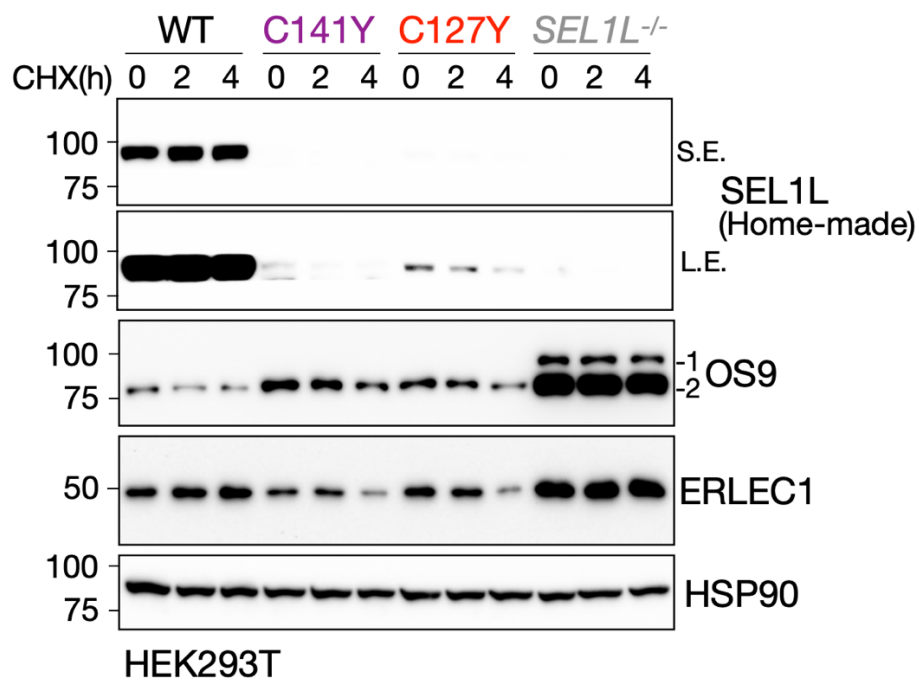


Supplemental Figure 5. ProAVP(G57S) aggregation and extended ER volume in *SEL1L*^{C141Y} cells. (A-B) Reducing and non-reducing SDS-PAGE and Western blot analyses of proAVP-G57S high molecular-weight (HMW) aggregates in various HEK293T cells, with quantitation of proAVP-G57S-HA HMW in (B) ($n = 3-4$ independent samples per group). *SEL1L*^{-/-} and *HRD1*^{-/-} HEK293T cells were included as a control and quantitated together as “ERAD KO”. (C) Representative confocal images of KDEL (red) in WT and *SEL1L*^{C141Y} patient fibroblasts. Two independent repeats. Data are presented as mean \pm SEM. n.s., not significant. **** $p < 0.0001$ by one-way ANOVA followed by Tukey’s pos hoc test (B).

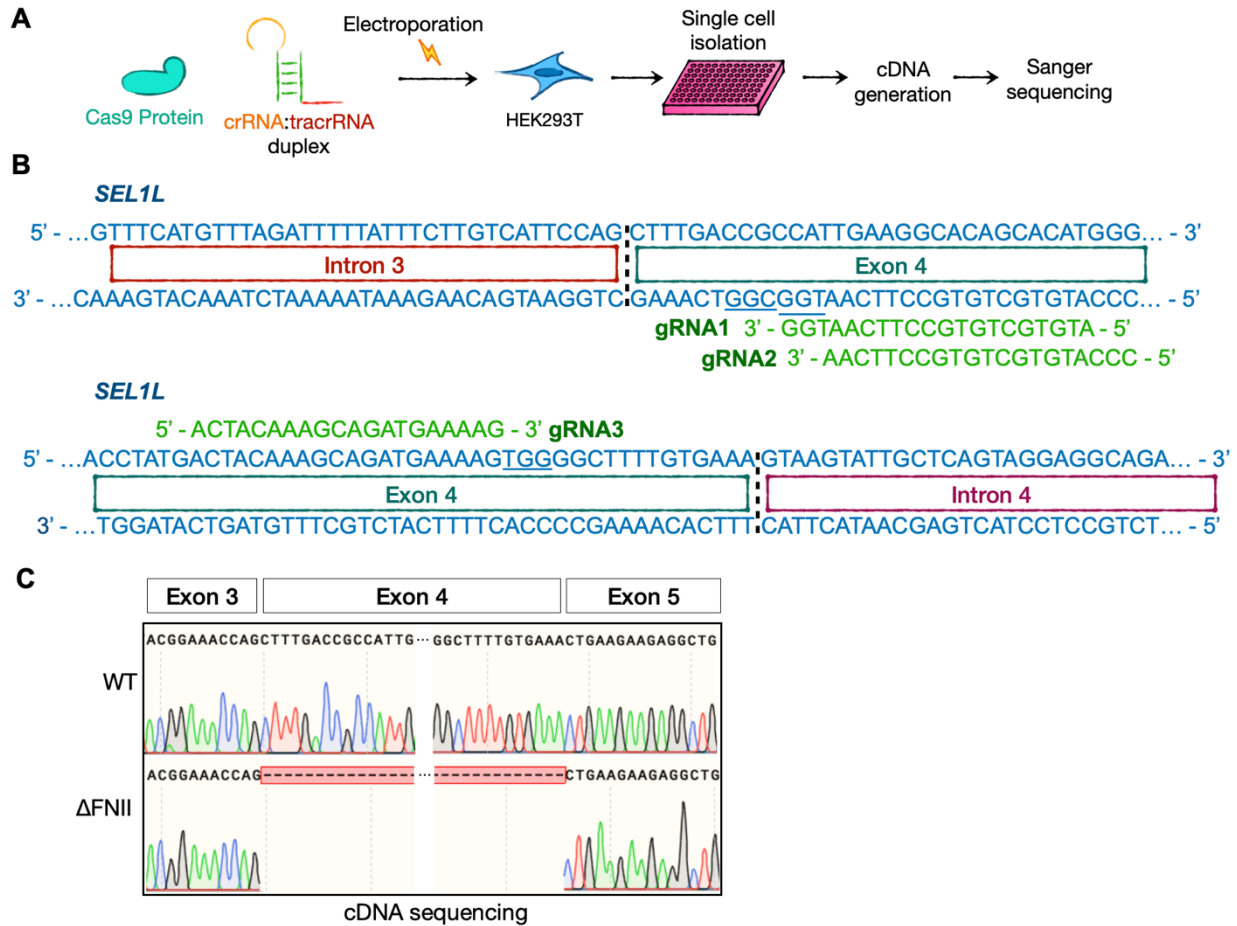


Supplemental Figure 6. Generation of knock-in (KI) HEK293T cells carrying the variants via CRISPR-Cas9 Homology Directed Repair (HDR) or Base editing (BE).

(A) Schematic diagram of the generation of *SEL1L* KI HEK293T cells using the CRISPR/Cas9 technology. (B) gRNA and ssDNA HDR template donor designs for *SEL1L* C141Y. PAM sites are underlined. (C) gRNA design for *SEL1L* C127Y. PAM site is underlined. (D-E) Sanger sequencing confirmation of *SEL1L* C141Y (D) and C127Y (E) KI HEK293T cells. The shaded red box and arrow indicated the mutations.

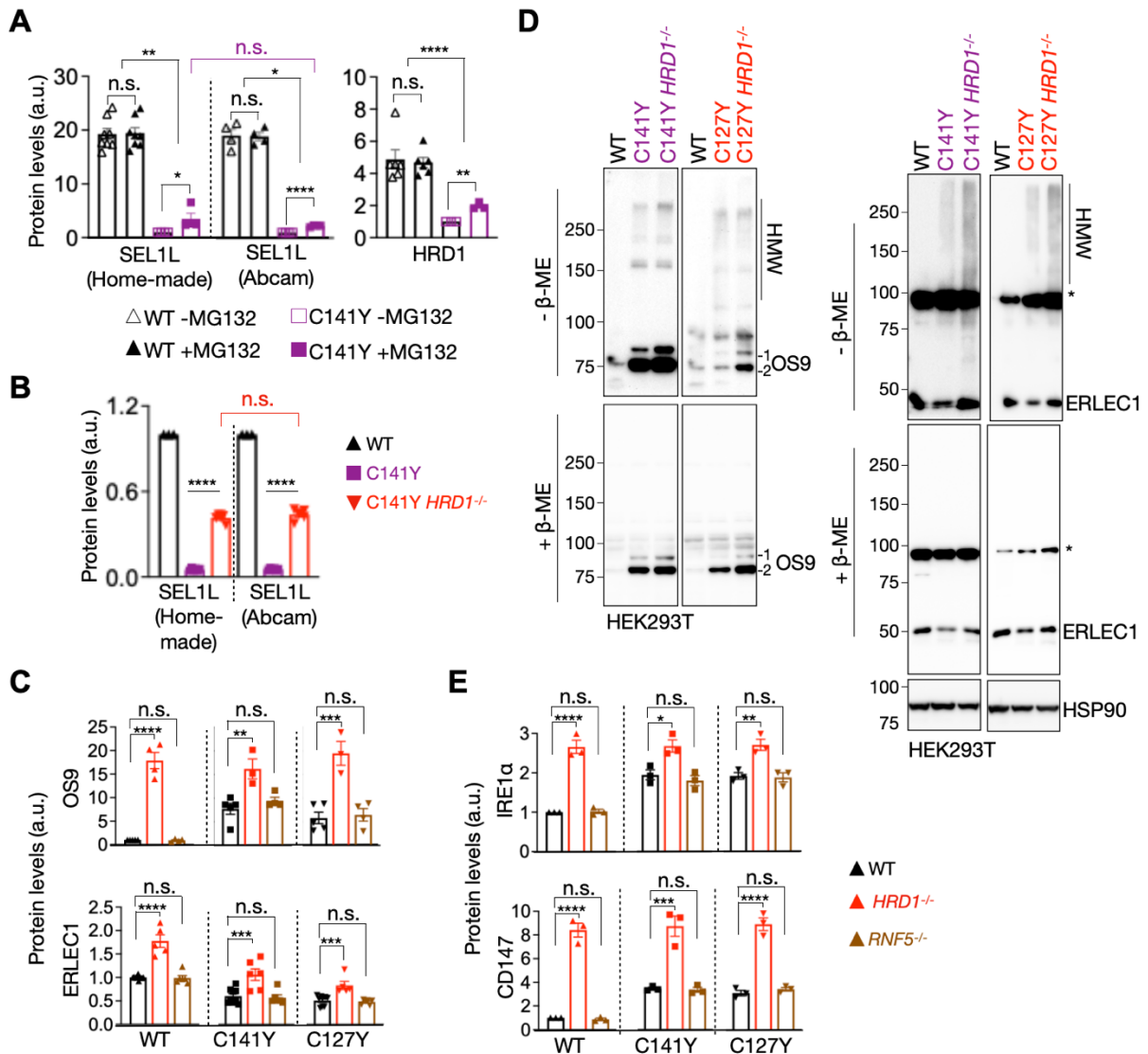


Supplemental Figure 7. Destabilization of OS9 and ERLEC1 in *SEL1L*^{C141Y} and *SEL1L*^{C127Y} KI HEK293T cells but not *SEL1L*^{-/-} HEK293T cells. Cycloheximide (CHX) chase analysis of ERAD proteins and endogenous ERAD substrates in HEK293T cells, with quantitation shown in Figure 5E (n = 5-6 independent samples per group).



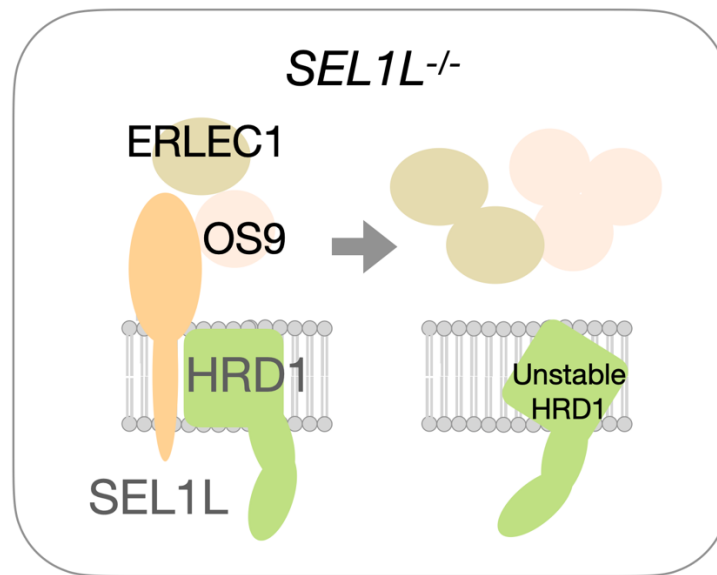
Supplemental Figure 8. Generation and validation of ΔFNII SEL1L knock-in (KI) HEK293T cells via CRISPR-Cas9.

(A) Schematic diagram of the generation of SEL1L ΔFNII KI HEK293T cells using the CRISPR/Cas9 technology. (B) gRNAs designs. PAM sites are underlined. (C) Sanger sequencing of cDNA samples confirming the deletion of exon 4, which encodes for the FNII domain.



Supplemental Figure 9. Turnover of SEL1L-HRD1 ERAD components in *SEL1L*^{C141Y} cells by HRD1, not RNF5.

(A) Quantitation of SEL1L and HRD1 proteins in WT and *SEL1L*^{C141Y} patient fibroblasts from Figure 7A (n = 6-8 and 3-4 independent samples for WT and C141Y). (B) Quantitation of SEL1L detected using different SEL1L antibodies in the KI HEK293T cells with/without *HRD1*^{-/-} from Figure 7D. (C) Quantitation of OS9, ERLEC1 from Figure 7B. (D) Reducing and non-reducing SDS-PAGE and Western blot analysis showing high molecular-weight (HMW) aggregation and HRD1-mediated degradation of OS9 and ERLEC1 in KI HEK293T cells (representative of two repeats). (E) Quantitation of IRE1α and CD147 from Figure 7B. Data are presented as mean ± SEM. n.s., not significant. *p<0.05, **p<0.01, ***p<0,001 and ****p<0.0001 by one-way ANOVA followed by Tukey's pos hoc test (A, B, C, E).



Supplemental Figure 10. A schematic illustrating SEL1L deficiency on ERAD components. In *SEL1L^{-/-}* cells, the absence of SEL1L attenuates the interaction between lectins OS9/ERLEC1 and HRD1, leading to their protein stabilization, while triggering auto-ubiquitination and self-degradation of HRD1.